J Mater Sci (2013) 48:644–650
DOI 10.1007/s10853-012-6768-5

Synthesis of $Y_2O_2S:Eu^{3+}$ luminescent nanobelts via electrospinning combined with sulfurization technique

Liying Yang · Jinxian Wang · Xiangting Dong · Guixia Liu · Wensheng Yu

Received: 19 May 2012 / Accepted: 25 July 2012 / Published online: 14 August 2012

Abstract $Y_2O_2S:Eu^{3+}$ nanobelts were successfully prepared via electrospinning method and sulfurization process using the as-prepared $Y_2O_3:Eu^{3+}$ nanobelts and sulfur powders as sulfur source by a double-crucible method for the first time. X-ray diffraction analysis indicated that the $Y_2O_2S:Eu^{3+}$ nanobelts were pure hexagonal in structure with space group $P\ \bar{3}m1$. Scanning electron microscope images showed that the width and thickness of the $Y_2O_2S:Eu^{3+}$ nanobelts were ca. 6.7 μm and 125 nm, respectively. Under the excitation of 325-nm ultraviolet light, $Y_2O_2S:Eu^{3+}$ nanobelts exhibited red emissions of predominant peaks at 628 and 618 nm, which are attributed to the $^5D_0 \rightarrow {}^7F_2$ transition of the Eu^{3+} ions. It was found that the optimum doping concentration of Eu^{3+} ions in the Y_2O_2S: Eu^{3+} nanobelts was 3 %. Compared with bulk particle, Eu^{3+}–O^{2-}/S^{2-} charge transfer bands (260 and 325 nm) of the $Y_2O_2S:Eu^{3+}$ nanobelts showed a blue-shift significantly. The formation mechanism of the Y_2O_2S: Eu^{3+} nanobelts was also proposed. This new sulfurization technique is of great importance, not only to inherit the morphology of rare earth oxides but also to fabricate pure-phase rare earth oxysulfides at low temperature compared with conventional sulfurization method.

Introduction

As a group of important wide-gap (4.6–4.8 eV) semiconductor materials, rare earth oxysulfides with high chemical and thermal stability have been extensively used as optical functional materials [1, 2], owing to their high absorption of light and efficient energy transfer. Among these materials, rare earth ions-activated lanthanide oxysulfides have become a very important family of inorganic phosphor materials [3], especially for $Y_2O_2S:Eu^{3+}$, one of the most efficient phosphors [4] that have wide applications in the fields of color television tubes, field emission display, and long-lasting phosphorescence. Recently, a large number of fabrication methods have already been employed to prepare micro- and nanosized $Y_2O_2S:Eu^{3+}$, such as hydrothermal and solvothermal method [5], solid-sate reaction method [6, 7], combustion method [8, 9], microwave-heating method [10, 11], etc. These methods led to produce $Y_2O_2S:Eu^{3+}$ nanoparticles [12], nanotubes, nanowires, nanorods [13], and nanoflowers [14]. However, rare earth oxysulfides nanobelts were limited. Therefore, fabrication of rare earth oxysulfides nanobelts is a meaningful subject of study.

Conventionally, $RE_2O_2S:Ln^{3+}$ (RE = Y, La, Gd; Ln = Eu, Tb) luminescent bulk materials were prepared by the calcination of the mixture of rare earth oxides [10, 11] or oxalate compounds [15, 16] or carbonates [17, 18], sulfur powders, and flux (Na_2CO_3, $Mg_2CO_3{\cdot}4\ Mg(OH)_2{\cdot}5H_2O$, TiO_2) at above 1,100 °C for 2 h in a reduced or protective atmosphere. In this way, the as-prepared bulk materials often have irregular morphology and cannot inherit the peculiar morphologies of rare earth oxide precursors because sulfur powders and flux will melt and destruct the morphologies of rare earth oxides. Therefore, it is difficult to obtain rare earth oxysulfide nanobelts via the conventional sulfurization method using rare earth oxide nanobelt as a precursor.

Electrospinning is a simple, convenient, and versatile technique to prepare long fibers with diameters ranging from tens of nanometers up to micrometers, including rare earth oxyfluoride nanofibers [19], rare earth oxide, and composite

L. Yang · J. Wang · X. Dong (✉) · G. Liu · W. Yu
Key Laboratory of Applied Chemistry and Nanotechnology at Universities of Jilin Province, Changchun University of Science and Technology, Changchun 130022, China
e-mail: dongxiangting888@163.com

oxide nanofibers and nanobelts [20–23]. However, to the best of our knowledge, there have been no reports on the preparation of rare earth oxysulfides nanobelts by electrospinning combined with sulfurization technique.

In this paper, $Y_2O_2S:Eu^{3+}$ nanobelts were fabricated through the sulfurization of the relevant $Y_2O_3:Eu^{3+}$ nanobelts which were prepared by the calcination of the electrospun belts of PVP/[$Y(NO_3)_3 + Eu(NO_3)_3$] composites. A sulfurization mechanism for the $Y_2O_2S:Eu^{3+}$ nanobelts was proposed. Finally, we investigated the photoluminescence properties of the $Y_2O_2S:Eu^{3+}$ nanobelts. This synthetic route is also suitable for fabricating other rare earth oxysulfide nanomaterials.

Experimental section

Chemicals

Polyvinyl pyrrolidone (PVP) (Mw = 90,000, AR), yttrium oxide (Y_2O_3) (99.99 %), and europium oxide (Eu_2O_3) (99.99 %) were purchased from Kemiou Chemical Co. Ltd. *N*,*N*-Dimethylformamide (DMF, AR) was bought from Tiantai Chemical Co. Ltd. Nitric acid (AR) and sulfur(AR) were purchased from Beihua Fine Chemical Co. Ltd. All chemicals were directly used as received without further purification.

Preparation of PVP/[$Y(NO_3)_3 + Eu(NO_3)_3$] composite nanobelts via electrospinning

Y_2O_2S:x % Eu^{3+} [x = 1,3,5,7, x stands for molar ratio of Eu^{3+} to ($Eu^{3+} + Y^{3+}$)] were prepared by an electrospinning method combined with sulfurization technique. In a typical procedure of preparing Y_2O_2S:3 %Eu^{3+}, rare earth nitrates were first prepared by dissolving 0.0382 g of Eu_2O_3 and 0.7913 g of Y_2O_3 in dilute HNO_3 (1:1, volume ratio) at elevated temperatures. Then, 13.9128 g of DMF was added into the rare earth nitrates, and a clear DMF solution was formed. Finally, 4 g of PVP was added into the above solution under stirring for 4 h to form homogeneous transparent precursor solution. In the precursor solution, the mass ratios of rare earth nitrates, DMF, and PVP were equal to 10:70:20. Subsequently, the precursor solution was electrospun at room temperature under a positive high voltage of 8 kV, the distance between the capillary tip and the collector (Al foil) was fixed to 15 cm, and relative humidity was 60 ~ 80 %. PVP/[$Y(NO_3)_3 + Eu(NO_3)_3$] composite nanobelts were obtained on the collector with the evaporation of DMF.

Preparation of $Y_2O_3:Eu^{3+}$ nanobelts

The as-prepared PVP/[$Y(NO_3)_3 + Eu(NO_3)_3$] composite nanobelts were annealed at 700 °C for 8 h with a heating rate of 1 °C/min. Then, the calcination temperature was decreased to 200 °C at a rate of 1 °C/min. Finally, samples were down to room temperature naturally and $Y_2O_3:Eu^{3+}$ nanobelts were obtained.

Fabrication of $Y_2O_2S:Eu^{3+}$ nanobelts

$Y_2O_2S:Eu^{3+}$ nanobelts were prepared by an Ar gas-aided sulfur treatment through calcining $Y_2O_3:Eu^{3+}$ nanobelts precursor using sulfur powder as a sulfurization agent. Some sulfur powders were put into a small crucible, the sulfur powders were covered by some carbon rods, and the $Y_2O_3:Eu^{3+}$ nanobelts were placed on the carbon rods. Next, this small crucible was put into a big crucible, some sulfur powders were loaded into the space between the two crucibles, and the big crucible was covered with the lid. We call this process as a double-crucible method. The crucibles were annealed at 800 °C for 4 h under Ar gas atmosphere at the heating rate of 5 °C/min. Then, the calcination temperature was decreased to 200 °C at a rate of 5 °C/min followed by decreasing it down to room temperature naturally. Thus, $Y_2O_2S:Eu^{3+}$ nanobelts were successfully acquired.

Synthesis of $Y_2O_2S:Eu^{3+}$ particles

For comparison, we prepared $Y_2O_2S:Eu^{3+}$ bulk particles through a conventional solid-state reaction method according to the Ref. [24]. The mean size of particles is ca. 6 μm.

Characterization methods

X-ray diffraction (XRD) measurements were carried out using a Rigaku D/max-RA XRD diffractometer with Cu Kα radiation of 0.15418 nm. The size and morphology of the products were observed by a field emission scanning electron microscope (FESEM, XL-30, FEI Company). The purity of the products was examined using OXFORD ISIS-300 energy dispersive spectrometer (EDS). Transmission electron microscope (TEM) analysis was performed using a JEM-2010 transmission electron microscope under a working voltage of 200 kV. The excitation and emission spectra of samples were recorded using a HITACHI F-7000 Fluorescence Spectrophotometer using a Xe lamp as the excitation source.

Results and discussion

XRD analysis

Figure 1 shows the XRD patterns of the as-prepared Y_2O_3:3 %Eu^{3+} nanobelts and Y_2O_2S:3 %Eu^{3+} nanobelts

with different doping concentration of Eu^{3+} ions. All the diffraction peaks of the Y_2O_3:3 %Eu^{3+} (Fig. 1a) can be readily indexed to those of the pure cubic phase with primitive structure of Y_2O_3 (PDF#43-0661), space group is $Fm\bar{3}m$. No other phases are identified. The reflection peaks of the Y_2O_2S:Eu^{3+} (Fig. 1b–e) can be perfectly indexed as the pure hexagonal phase of Y_2O_2S (PDF#24-1424), space group is $Pm\bar{3}1$. No diffraction peaks of any other phases or impurities are also detected. These results indicate that the pure-phase Y_2O_3:Eu^{3+} could be obtained after the PVP/[$Y(NO_3)_3$ + $Eu(NO_3)_3$] composite were calcined at 700 °C for 8 h and the hexagonal Y_2O_2S:Eu^{3+} were acquired via the sulfurization of the cubic Y_2O_3:Eu^{3+} at 800 °C for 4 h. The doping of Eu^{3+} did not change the Y_2O_2S host lattice structure.

SEM, TEM, and EDS analysis

Figure 2a shows the typical SEM image of PVP/[$Y(NO_3)_3$ + $Eu(NO_3)_3$] composite before calcinations. One can see that the composite is composed of nanobelts with smooth surface and uniform width, indicating the formation of nanobelt. After annealing at 700 °C, these nanobelts experience about 70 % reduction in width due to loss of the PVP and associated organic components [22], as shown in Fig. 2b. The obtained Y_2O_3:3 %Eu^{3+} nanobelts still have smooth surface. Figure 2c shows the SEM image of the Y_2O_2S:3 %Eu^{3+} nanobelts. It reveals that morphology and the widths of Y_2O_2S:3 %Eu^{3+} nanobelts are nearly similar to those of Y_2O_3:3 %Eu^{3+} nanobelts. Preliminarily, we can conclude that the sulfur atmosphere plays an important role in keeping the morphology of the nanobelts. The thickness of Y_2O_2S:3 %Eu^{3+} nanobelts becomes thinner due to the decomposition of the organic species and the formation of inorganic phase. The thickness of PVP/[$Y(NO_3)_3$ + $Eu(NO_3)_3$] composite nanobelts, Y_2O_3:3 %Eu^{3+} nanobelts, and Y_2O_2S:3 %Eu^{3+} nanobelts are 494, 172, and 125 nm, respectively. Under the 95 % confidence level, the widths of those nanobelts analyzed by Shapiro–Wilk method are normally distributed. Histograms of widths of these belts are shown in Fig. 3. The widths of PVP/[$Y(NO_3)_3$ + $Eu(NO_3)_3$] composite nanobelts, Y_2O_3:3 %Eu^{3+} nanobelts, and Y_2O_2S:3 %Eu^{3+} nanobelts are 7.2 ± 0.6, 6.6 ± 0.5, and 6.7 ± 0.6 μm, respectively.

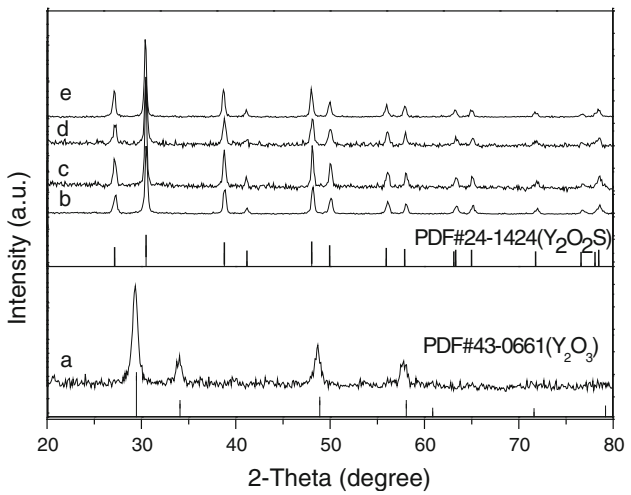

Fig. 1 XRD patterns of Y_2O_3:3 %Eu^{3+} nanobelts (*a*) and Y_2O_2S: x %Eu^{3+} [x = 1(*b*), 3(*c*), 5(*d*), 7(*e*)] nanobelts with PDF standard cards of Y_2O_3 (43-0661) and Y_2O_2S(24-1424)

Figure 4a illustrates TEM images of the Y_2O_2S:3 %Eu^{3+} nanobelts. It indicates that the nanobelts composed of nanoparticles with size of 10–30 nm. The corresponding selected area electron diffraction (SAED) patterns in Fig. 4b exhibit typical polycrystal diffraction patterns and are in good agreement with those of pure Y_2O_2S phase. These results further confirm the formation of the Y_2O_2S:Eu^{3+} nanobelts.

EDS spectrum of the Y_2O_2S:3 %Eu^{3+} nanobelts (Fig. 5) reveals the presence of Y, O, S, and Eu elements, and no other impurity elements including carbon, indicating that the pure Y_2O_2S:3 %Eu^{3+} nanobelts are obtained. Au peak is from the conductive film of Au plated on the sample for SEM observation.

Photoluminescence properties

Figure 6 illustrates the excitation (monitored by 628 nm) and emission (excited by 325 nm) spectra of the different Y_2O_2S:Eu^{3+} nanobelts. It is found from Fig. 6a that there

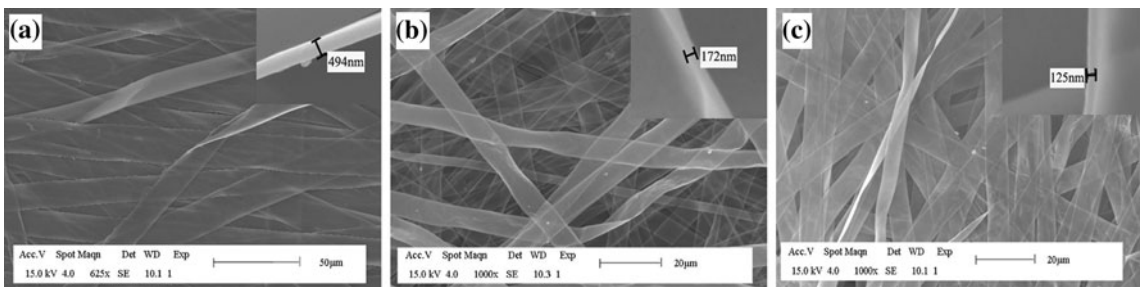

Fig. 2 SEM images of PVP/[$Y(NO_3)_3$ + $Eu(NO_3)_3$] **a** Composite nanobelts, **b** Y_2O_3:3 %Eu^{3+} nanobelts, and **c** Y_2O_2S:3 %Eu^{3+} nanobelts

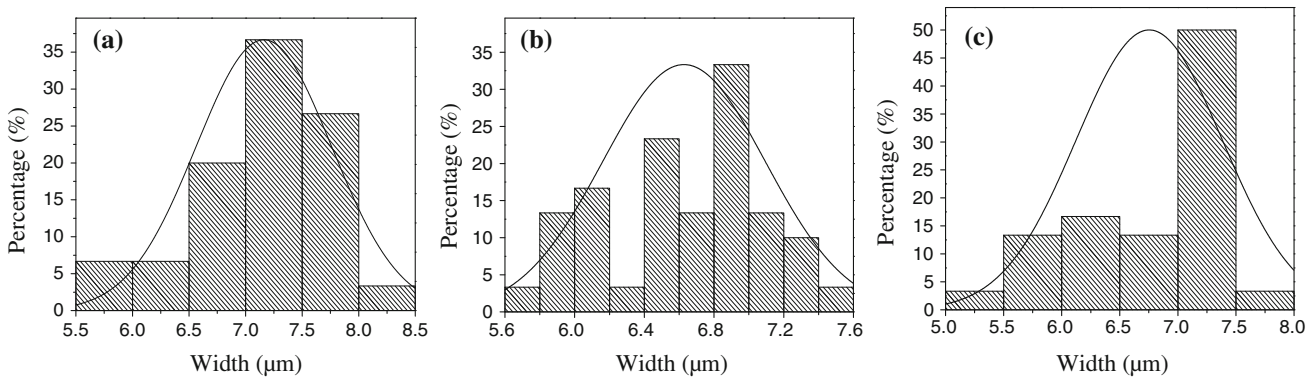

Fig. 3 Histograms of widths of PVP/[$Y(NO_3)_3$ + $Eu(NO_3)_3$] **a** Composite nanobelts, **b** Y_2O_3:3 %Eu^{3+} nanobelts, and **c** Y_2O_2S:3 %Eu^{3+} nanobelts

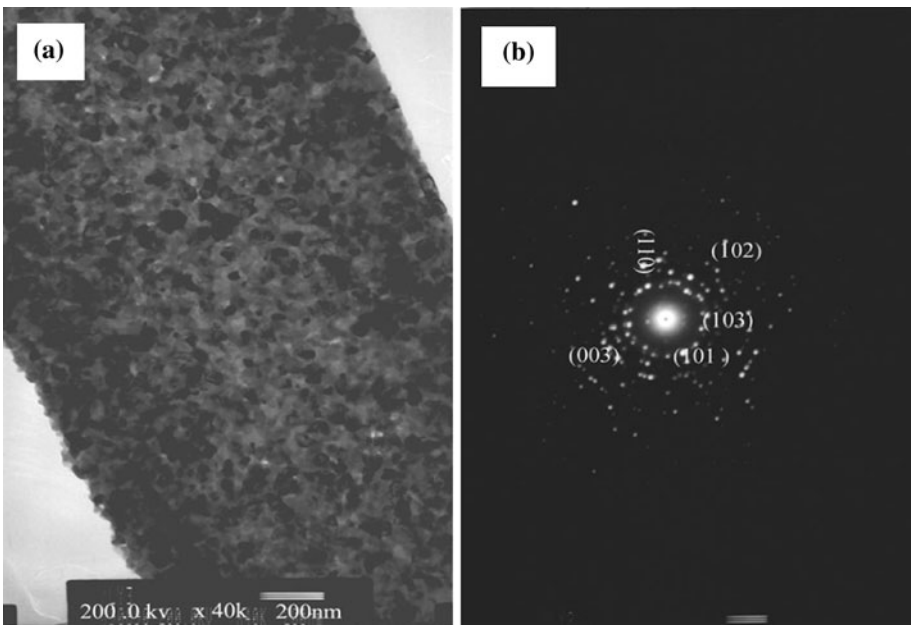

Fig. 4 **a** TEM image and **b** SAED pattern of Y_2O_2S:3 %Eu^{3+} nanobelts

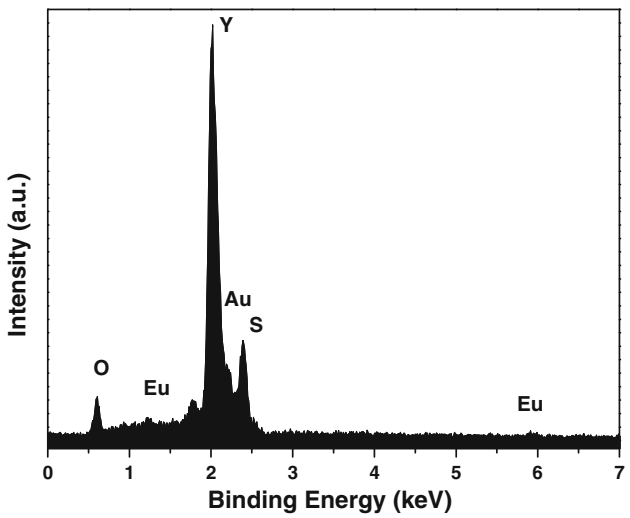

Fig. 5 EDS spectrum of Y_2O_2S:3 %Eu^{3+} nanobelts

is a wide band with two peaks at 260 and 325 nm, which are attributed to Eu^{3+}–O^{2-} CTB (charge transfer band) and Eu^{3+}–S^{2-} CTB, respectively. In the longer wavelength region (400–500 nm), the f–f transition peaks of the Eu^{3+} ions can be observed with very weak intensity compared with those of the CTB. The strongest intensity of the excitation spectrum (CTB) is obtained when the doping concentration of Eu^{3+} ion is 3 %. The matrix absorption band at 247 nm is also observed.

Figure 6b demonstrates the emission spectrum of the Y_2O_2S nanobelts doped with various concentration of Eu^{3+}. When the Eu^{3+} content is greater than 3 %, the concentration quenching effect occurs, as shown in the Fig. 7. At this time, the bond length between Eu^{3+} and O^{2-} becomes shorter and the mixture of wave function of Eu^{3+} and O^{2-} is enhanced [25], therefore, shows the strongest luminescence at 3 %. It is remarkably seen that the main emission peaks between 550 and 650 nm are observed from Fig. 6b, which

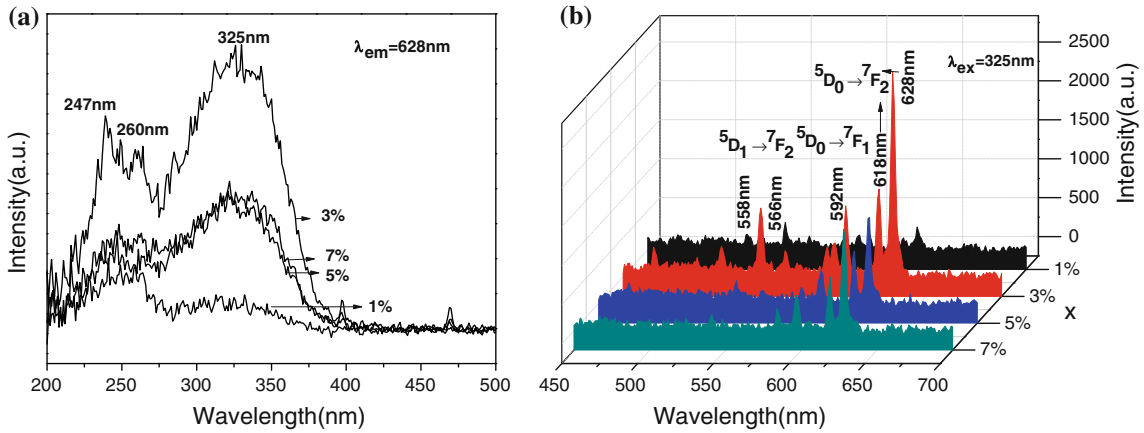

Fig. 6 **a** Excitation and **b** emission spectra of Y_2O_2S:x Eu^{3+} (x = 1, 3, 5, 7 %) nanobelts

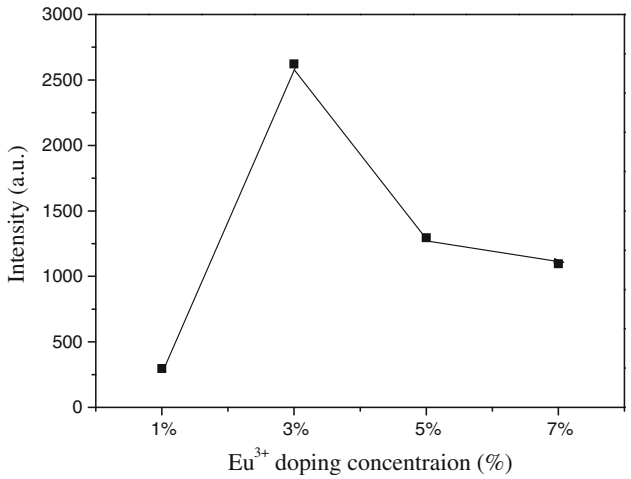

Fig. 7 Change of the emission intensity of peak at 628 nm ($^5D_0 \rightarrow {}^7F_2$) with Eu^{3+} doping concentrations

is in agreement with the results reported by Kader and Elkholy [26]. The emission spectrum is associated with the transitions from the excited level of the ^5D_J ($J = 0, 1$) to the level of ^7F_J ($J = 1, 2$) of the Eu^{3+} ions. The strongest red emission split into two peaks at 628 nm and 618 nm are ascribed to the $^5D_0 \rightarrow {}^7F_2$ transition of the Eu^{3+} ions, indicating that non-Y_2O_3 phase exists and the oxysulfide host has been formed [26]. Among several luminescence transitions of Eu^{3+} ion, the $^5D_0 \rightarrow {}^7F_1$ ($\sim$ 592 nm) is mainly a magnetic-dipole transition, while the $^5D_0 \rightarrow {}^7F_2$ ($\sim$628 nm) is an electric-dipole transition which is closely related to the coordination environment around Eu^{3+}. The stronger $^5D_0 \rightarrow {}^7F_2$ transition suggests that the Eu^{3+} ions occupy the sites at low symmetries without inversion center since this transition is hypersensitive to crystal structure and chemical surroundings [11, 27, 28]. The other emission peaks at 558 and 566 nm are attributed to the electron transition from the $^5D_1$ to $^7F_2$ level of the Eu^{3+} ions. It is clearly indicated from these emissions that the Eu^{3+} ions have been effectively distributed into the Y_2O_2S matrix.

Compared with the Y_2O_2S:Eu^{3+} bulk particles, the excitation bands (Eu^{3+}–O^{2-}/S^{2-}CTB) in the Y_2O_2S:Eu^{3+} nanobelts show apparent blue-shift, as shown in Fig. 8a.

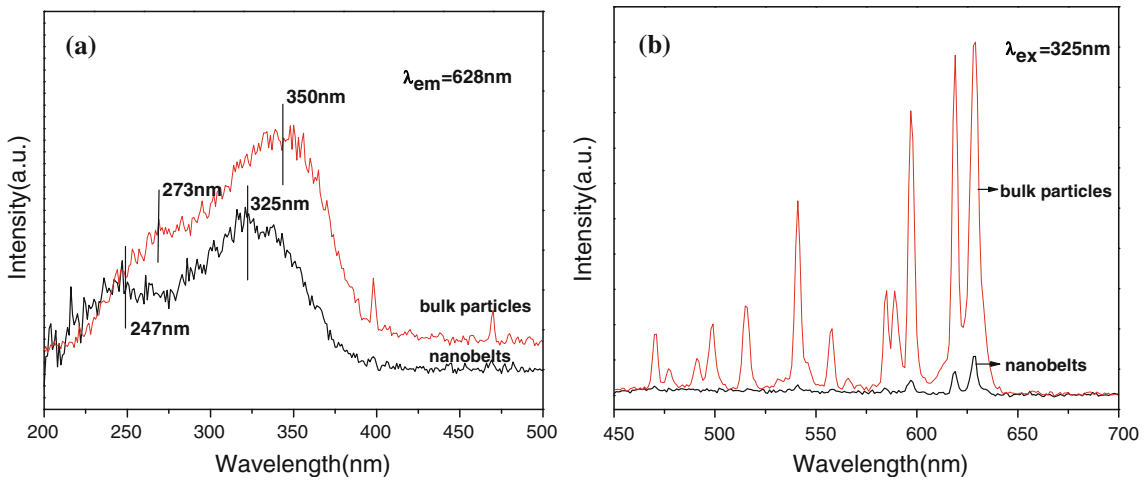

Fig. 8 **a** Excitation and **b** emission spectra of Y_2O_2S:3 %Eu^{3+} bulk particles and nanobelts

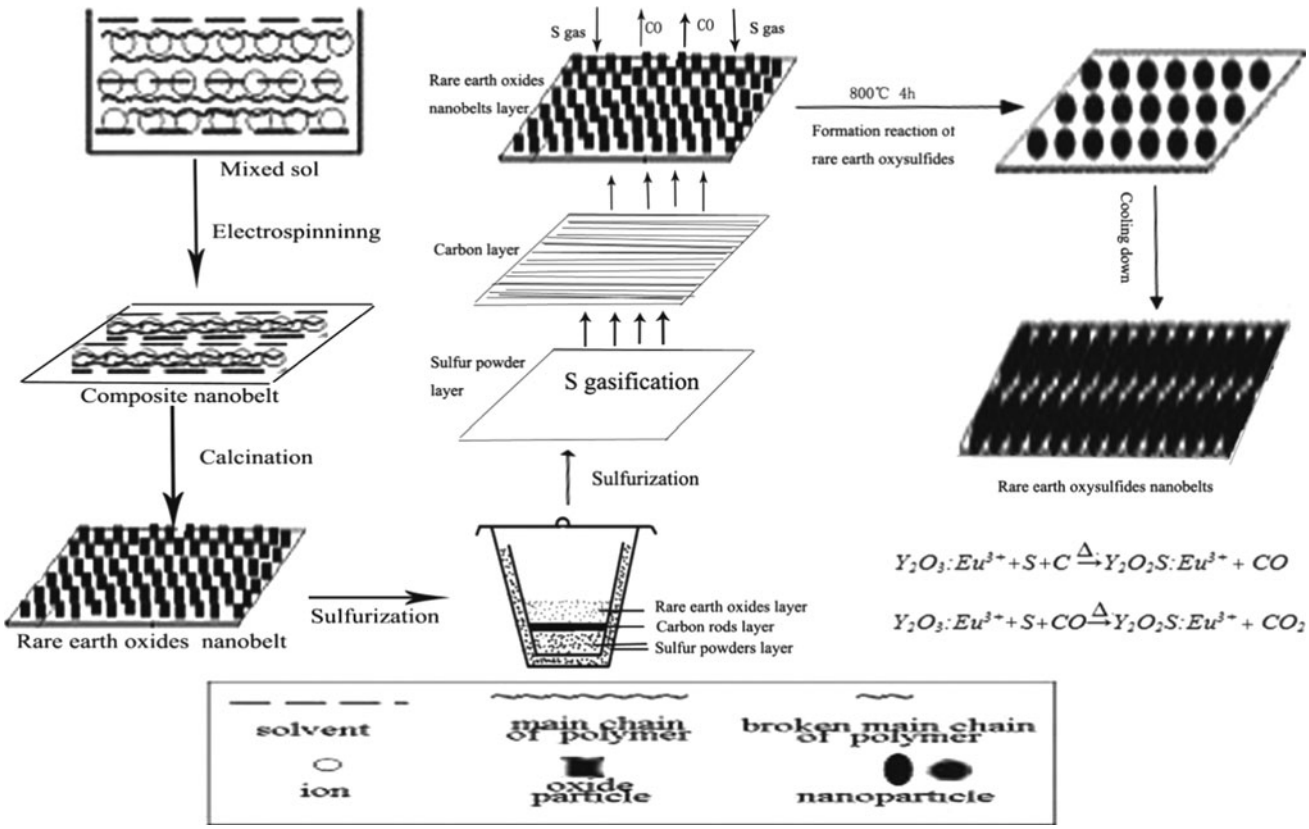

Fig. 9 Formation mechanism of $Y_2O_2S:Eu^{3+}$ nanobelt

This result can be possibly explained by size-dependent changes associated with quantum confinement effect in this wide-gap semiconductor materials [18]. Figure 8b shows emission spectra of the $Y_2O_2S:Eu^{3+}$ bulk particles and the $Y_2O_2S:Eu^{3+}$ nanobelts; it is clearly seen that the emission intensity of bulk particles is obviously stronger than that of nanobelts due to more surface defects of the $Y_2O_2S:Eu^{3+}$ nanobelts. All results are in good agreement with that of the Ref. [29, 30].

Formation mechanism for the $Y_2O_2S:Eu^{3+}$ nanobelts

Formation mechanism of $Y_2O_2S:Eu^{3+}$ nanobelt is shown in Fig. 9. PVP, $Y(NO_3)_3$, and $Eu(NO_3)_3$ were mixed with DMF to form precursor solution. Y^{3+}, Eu^{3+}, and NO_3^- were mixed or absorbed onto PVP to form sol with certain viscosity. Then, PVP/$[Y(NO_3)_3 + Eu(NO_3)_3]$ composite nanobelts were fabricated via electrospinning. PVP acted as template during the formation of $Y_2O_3:Eu^{3+}$ nanobelts. In the process of calcination, PVP was oxidized to break the chain and then to volatilize. Nitrates were decomposed and oxidized to produce NO_2, and Y^{3+}/Eu^{3+} was oxidized to form $Y_2O_3:Eu^{3+}$ crystallites; many crystallites were combined into nanobelt. In the sulfurization process, $Y_2O_3:Eu^{3+}$ nanobelt was sulfurized using S as a sulfurization agent and S was gasified at about 350 °C. With the increase of calcination temperature, gasified sulfur reacts with $Y_2O_3:Eu^{3+}$ nanobelts to produce $Y_2O_2S:Eu^{3+}$ nanobelt. During the reaction process, sulfur powders and $Y_2O_3:Eu^{3+}$ nanobelts were separated by carbon rods which prevented $Y_2O_3:Eu^{3+}$ nanobelts from the morphology damage and also played a key role in reduction through reacting with oxygen species of $Y_2O_3:Eu^{3+}$ in the heating process. The double-crucible method we proposed here is actually a solid–gas reaction, which has been proved to be an important method, not only can retain the morphology of the $Y_2O_3:Eu^{3+}$ nanobelts but also can fabricate the $Y_2O_2S:Eu^{3+}$ nanobelts with pure phase at relatively low temperature. Reaction schemes for the formation of the $Y_2O_2S:Eu^{3+}$ nanobelts proceed as follows:

$$\mathrm{PVP}/\left[\mathrm{Y(NO_3)_3} + \mathrm{Eu(NO_3)_3}\right] + \mathrm{O_2} \rightarrow \mathrm{CO_2} + \mathrm{H_2O} + \mathrm{NO_2} + \mathrm{Y_2O_3{:}Eu^{3+}} \quad (1)$$

$$\mathrm{Y_2O_3{:}Eu^{3+}} + \mathrm{S} + \mathrm{C} \xrightarrow{800\,^{\circ}\mathrm{C}} \mathrm{Y_2O_2S{:}Eu^{3+}} + \mathrm{CO} \quad (2)$$

$$\mathrm{Y_2O_3{:}Eu^{3+}} + \mathrm{S} + \mathrm{CO} \xrightarrow{800\,^{\circ}\mathrm{C}} \mathrm{Y_2O_2S{:}Eu^{3+}} + \mathrm{CO_2} \quad (3)$$

Conclusions

In summary, pure hexagonal phase $Y_2O_2S:Eu^{3+}$ nanobelts with space group $P\bar{3}m1$ were fabricated via the sulfurization of the cubic $Y_2O_3:Eu^{3+}$ nanobelts. The morphology of the $Y_2O_3:Eu^{3+}$ nanobelts precursor can be inherited to $Y_2O_2S:Eu^{3+}$ nanobelts using sulfur powders as sulfurization reagent via a double-crucible method. The width and thickness of the $Y_2O_2S:Eu^{3+}$ nanobelts are 6.7 ± 0.6 μm and 125 nm, respectively. PL measurements demonstrate the strongest emission peak is at 628 nm, originating from the $^5D_0 \rightarrow {}^7F_2$ transition of the Eu^{3+} ions, indicating that the Eu^{3+} ions occupy a site without inversion center in the $Y_2O_2S:Eu^{3+}$ nanobelts. The strongest luminescence is obtained when doping concentration of Eu^{3+} is 3 %. Compared with $Y_2O_2S:Eu^{3+}$ bulk particles, the $Y_2O_2S:Eu^{3+}$ nanobelts show a significant blue-shift in Eu^{3+}–O^{2-}/S^{2-} CTB. The double-crucible method proposed here is of great importance. This technique can be employed to fabricate rare earth oxysulfide nanomaterials with various morphologies.

Acknowledgments This work was financially supported by the National Natural Science Foundation of China (NSFC 50972020, 51072026), Ph.D. Programs Foundation of the Ministry of Education of China (20102216110002,20112216120003), the Science and Technology Development Planning Project of Jilin Province (Grant Nos. 20070402, 20060504), and Key Research Project of Science and Technology of Ministry of Education of China (Grant No. 207026).

References

1. Mikami M, Oshiyama A (1998) Phys. Rev. B 57:8939–8944
2. Jüstel T, Nikol H, Ronda C (1998) Angew Chem Int Ed 37: 3084–3103
3. Lian JB, Sun XD, Li JG, Li XD (2011) Opt Mater 33:596–600
4. Cavouras D, Kandarakis I, Nomicos CD, Bakas A, Panayiotakis GS (2000) Radiat Meas 32:5–13
5. Jiang Y, Wu Y, Xie Y, Qian YT (2000) J Am Ceram Soc 83: 2628–2630
6. Lo CL, Duh JG, Chiou BS, Peng CC, Ozawa L (2001) Mater Chem Phys 71:179–189
7. Chou TM, Mylswamy S, Liu RS, Chuang SZ (2005) Solid State Commun 136:205–209
8. Luo XX, Cao WH, Xing MM (2006) J Rare Earths 24:20–24
9. Dai QL, Song HW, Wang MY, Bai X, Dong B, Qin RF, Qu XS, Zhang H (2008) J Phys Chem C 112:19399–19404
10. Li YY, DC D, Cai SH (1996) J Rare Earths 14:16–20
11. Kim H, Hang DW, Lee JS (2004) J Am Chem Soc 126: 8912–8913
12. Song YH, You HP, Huang YJ, Yang M, Zheng YH, Zhang LH, Guo N (2010) Inorg Chem 49:11499–11504
13. Li WY, Liu YL, Ai PF, Chen XB (2009) J Rare Earths 27: 895–899
14. Thirumalai J, Chandramohan R, Vijayan TA, Somasundaram RM (2011) Mater Res Bull 46:285–291
15. Wang F, Yang B, Zhang JC, Dai YN, Ma WH (2010) J Lumin 130:473–477
16. Pires AM, Serra OA, Davolos (2004) J Alloy Compd 374: 181–184
17. Ai PF, Li WY, Xiao LY, Li YD, Wang HJ, Liu YL (2010) Ceram Int 36:2169–2174
18. Fu Y, Cao WH, Peng Y, Luo XX, Xing MM (2010) J Mater Sci 45:6556–6561. doi:10.1007/s10853-010-4744-5
19. Wang HY, Yang Y, Wang Y, Zhao YY, Li X, Wang C (2009) J Nanosci Nanotechnol 9:1522–1525
20. Wang JX, Che HR, Dong XT, Liu L, Liu GX (2010) Acta Optica Sinica 30:473–479
21. Liu Y, Wang JX, Dong XT, Liu GX (2010) Chem J Chin Univ 31:1291–1296
22. Dong XT, Liu L, Wang JX, Liu GX (2010) Chem J Chin Univ 31:20–25
23. Cui QZ, Dong XT, Wang JX, Li M (2008) J Rare Earths 26:664–669
24. Lei BF, Liu YL, Zhang JW, Meng JX, Man SQ, Tan SZ (2010) J Alloy Compd 495:247–253
25. Xu L, Song HW, Dong B, Wang Y, Bai X, Wang GL, Liu Q (2009) J Phys Chem C 113:9609–9615
26. Kader AA, Elkholy MM (1990) Chem Mater Sci 1:95–99
27. Chou TW, Mylswamy S, Liu RS, Chuang SZ (2005) Solid State Commun 136:205–209
28. Thirumalai J, Chandramohan R, Divakar R, Mohandas E, Sekar M, Parameswaran P (2008) Nanotechnology 19:455–458
29. Blasse G (1976) Chem Mater Sci 26:43–79
30. Nakkiran A, Thirumalai JM, Jagannathan R (2007) Chem Phys Lett 436:155–161